

The optical design of the G-CLEF Spectrograph: the first light instrument for the GMT

Sagi Ben-Ami^a, Harland Epps^b, Ian Evans^a, Mark Mueller^a, William Podgorski^a, Andrew Szentgyorgyi^a

^aHarvard-Smithsonian Center for Astrophysics, 60 Garden St., Cambridge, MA 02140;

^bUCO/Lick Observatory, University of California, Santa Cruz, CA 95064

ABSTRACT

The GMT-Consortium Large Earth Finder (G-CLEF), the first major light instrument for the GMT, is a fiber-fed, high-resolution echelle spectrograph. In the following paper, we present the optical design of G-CLEF. We emphasize the unique solutions derived for the spectrograph fiber-feed: the Mangin mirror that corrects the cylindrical field curvature, the implementation of VPH grisms as cross dispersers, and our novel solution for a multi-colored exposure meter. We describe the spectrograph blue and red cameras comprised of 7 and 8 elements respectively, with one aspheric surface in each camera, and present the expected echellogram imaged on the instrument focal planes. Finally, we present ghost analysis and mitigation strategy that takes into account both single reflection and double reflection back scattering from various elements in the optical train.

Keywords: GMT, ELT, Echelle, Spectrographs, PRV, Exoplanets.

1. INTRODUCTION

The GMT-Consortium Large Earth Finder (G-CLEF) is a fiber-fed, high-resolution echelle spectrograph for the Giant Magellan Telescope (GMT). G-CLEF, to be commissioned in 2022, will be the first major instrument to go on the GMT. G-CLEF covers a wide wavelength range, from 350-950nm, and implements an asymmetric white pupil design (*e.g.*, [1,2]). Large format CCDs and a dichroic, which separate the dispersed beam into two channels, blue (350-540nm) and red (540-950nm), allow G-CLEF to cover its entire wavelength range in a single exposure.

G-CLEF is located inside a vacuum chamber, which is thermally stabilized and is mounted on a gravity invariant platform of the GMT. It is fed by a novel fiber-slit that allows observations at several resolutions: two high-resolution pupil-sliced modes with precision radial velocity measurements capabilities (PRV and non-scrambled PRV; $\mathcal{R} = 108,000$), each using seven 100 μm core fibers, a medium resolution mode (MR; $\mathcal{R} = 35,000$) using 300 μm core fibers, a high throughput mode (HT; $\mathcal{R} = 19,000$) using 450 μm core fibers, and a Multi-Object Spectrograph (MOS) mode using the GMT Many Instrument Fiber System (MANIFEST) interface [3].

A preliminary design review (PDR) was convened in April 2015. An overview of the innovative features of G-CLEF post-PDR design as well as a detailed discussion of G-CLEF opto-mechanical design, structure analysis, software development, and flexure control camera are provided in other submissions to these proceedings [4-8].

In the following paper we present the optical design of G-CLEF. This design is a re-optimization of the G-CLEF spectrograph design in response to PDR panel comments. The design presented at PDR is discussed in [9]. We emphasize some of the unique solutions that allow G-CLEF to deliver excellent performance for the various operational modes implemented to enable key science programs. Section 2 gives a detailed description of the optical layout, from the telescope feed, through focal ratio converters inside the spectrograph enclosure, the spectrograph *common path*¹, and the blue and red arms (*i.e.*, cross dispersers and spectrograph cameras). Section 3 describes the final echellograms imaged on the instrument focal plane, while section 4 describes our novel solution for a multi-colored exposure meter. Detailed ghost analysis and mitigation strategies, including Mangin mirror single-reflection ghosts,

¹ We call the part of the spectrograph before the beam is split to red/blue arm by the dichroic the spectrograph *common path*.

VPH recombination and Littrow ghosts, and camera pupil and focused ghosts, are given in section 5. Finally, a summary is given in section 6.

2. OPTICAL LAYOUT

The G-CLEF spectrograph optical layout is an asymmetric white pupil echelle design, Fig. 1 and Table 1.

Table 1: G-CLEF general parameters.

Wavelength	350-950nm
Diff. orders	65-175
Fiber F/#	3
Spectrograph F/#	8
Beam Dia. (Grating)	300mm
Beam Dia. (White Pupil)	200mm
Dichroic Split	540nm
Camera Focal length	450mm

In the following section we describe the optical layout of the various subsystems. In general, light is injected to the spectrograph through a novel fiber feed, collimated by an off-axis parabolic mirror (M1) onto an echelle grating mosaic that disperses the beams back towards M1. In 2nd pass, the rays are reflected by M1 towards a Mangin mirror and onto the pupil transfer mirror (M2) that collimates the light once again. A dichroic reflects/transmits light to blue/red arms, in which the slit monochromatic images are imaged on a large format monolithic CCD. A detailed description of the instrument front-end optics will be published in [10].

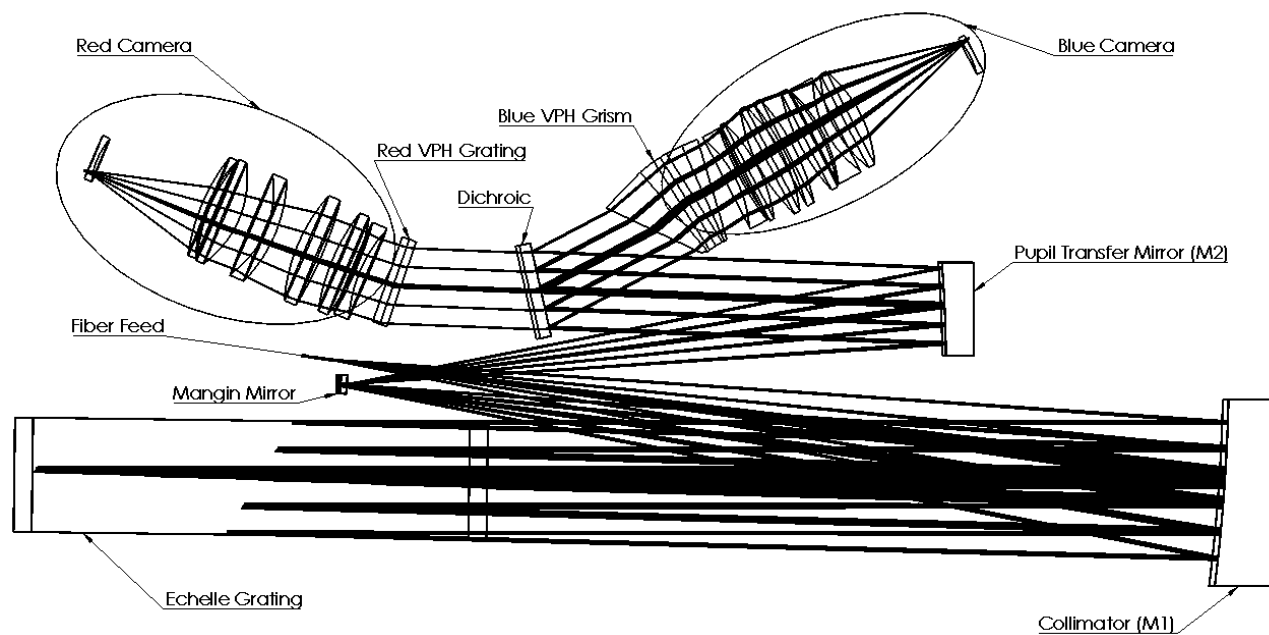


Figure 1: G-CLEF Optical Layout.

2.1 Fiber feed

As mentioned in the introduction, G-CLEF will operate at various resolutions, from $R=19,000$ to $R=108,000$. The fiber utilized in a given observation determines the resolution in a specific exposure (*i.e.*, the fiber core diameter), as listed in Table 2.

Table 2: G-CLEF Resolution Modes: Precision Radial Velocity (PRV), Non Scrambled Precision Radial Velocity (NS-PRV), Medium Resolution (MR), and High Throughput (HT).

Mode	Resolution	Fiber	#Science Fibers	#Calib/Sky Fibers	Comments
PRV	108,000	Hexagonal 100µm Core	7	2	Precision Radial Velocity
NS-PRV	108,000	Circular 100µm Core	7	2	Non-Scramble PRV
MR	35,000	Circular 300µm Core	1	2	Medium Resolution
HT	19,000	Circular 450µm Core	1	2	High Throughput

While the GMT operates at F/8, the focal ratio degradation inherent in all optical fibers is minimized when fibers are fed at an F/3. We therefore use a focal reducer comprised of two doublets to convert the beam from the native F/8 of the telescope to F/3 native to the optical fibers, Fig. 2.

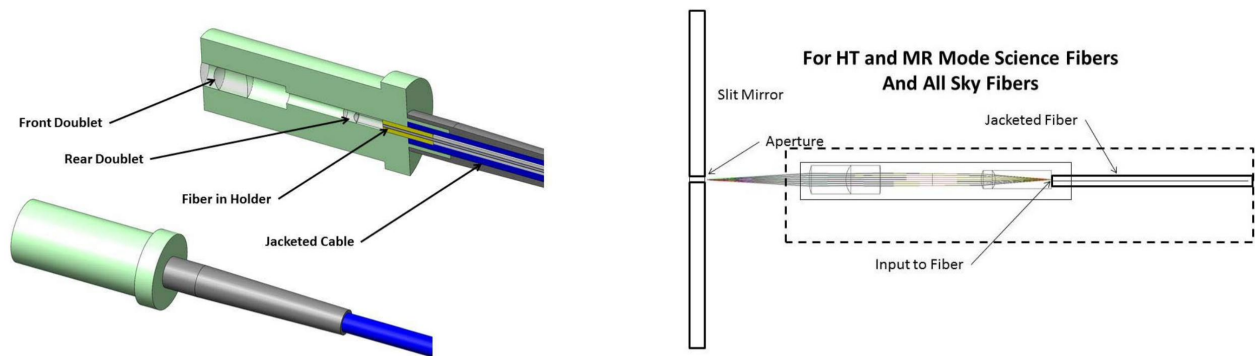


Figure 2: MR/HT modes fiber feed.

In the case of the PRV modes, since the resolution of a spectrograph is proportional the ratio of the beam diameter at the spectrograph collimator (d_{col}) to the primary mirror diameter (D_{tel}):

$$\mathcal{R} \propto \frac{d_{col}}{D_{tel}},$$

we need to slice the telescope beam to keep optical element diameters downstream of reasonable size. This is achieved by reimaging the telescope pupil using a doublet collimating lens and feeding the beam from each of the seven GMT mirror pairs to 100µm fibers (*i.e.*, slicing the telescope pupil to seven independent beams). The advantage of a pupil slicer over an image slicer is a uniform illumination of the spectrograph grating downstream to all sliced beams. The pupil slicer also converts the F/8 beam from the telescope to an F/3 beam to reduce focal ratio degradation, with the fibers cemented directly to the last lens in order to reduce the number of air-to-glass interfaces, see Fig. 3 and Table 3.

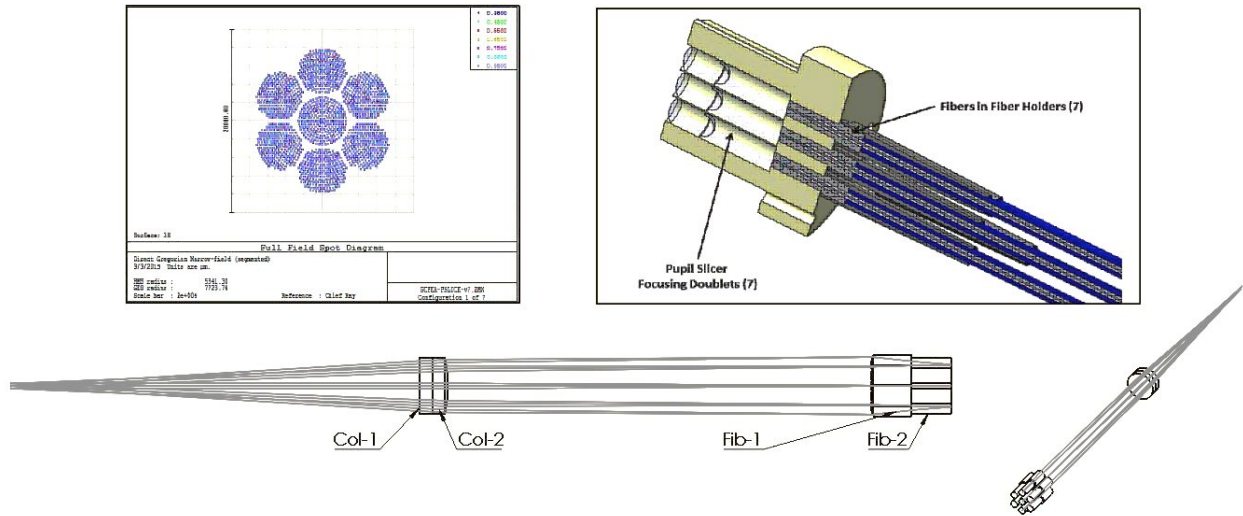


Figure 3: Reimaged GMT Pupil footprint and the Pupil Slicer Layout.

Table 3: Pupil Slicer Optical Prescription.

Element	RoC S1 [mm]	RoC S2 [mm]	Thickness [mm]	Air Space [mm]	Glass Type	Diameter [mm]
Col-1	Infinity	42.16Cc	3	Cemented to Col-2	BAL35Y	15.8
Col-2	42.16Cx	39.17Cx	5	117.81	CaF2	15.8
Fib-1	5.02Cx	2.20Cx	8.87	Cemented To Fib-2	CaF2	5.5
Fib-2	2.20Cc	Infinity	12	20.724	BAL15Y	5.5

2.2 Spectrograph common path

The light enters the spectrograph from the optical fiber slit at F/3. The chief rays are aimed at a 7.5-degree tilt with respect to the optical axis of the parabolic mirror M1. The output focal ratio of the fiber is converted to F/8 by a finite-conjugate lens system (focal ratio converter) with a telecentric image space, see Fig. 4 and Table 4.

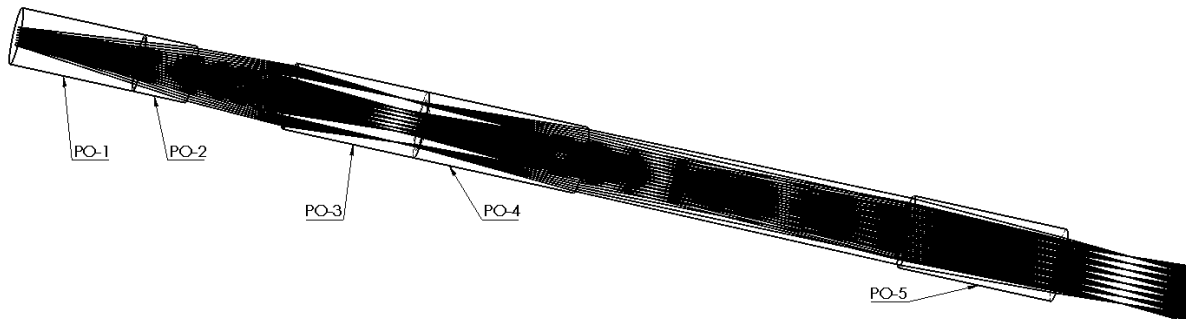


Figure 4: Focal Ratio Converters. The fibers are cemented to the flat surface of the 1st lens.

Table 4: Focal Ratio Converters Optical Prescription.

Element	RoC S1 [mm]	RoC S2 [mm]	Thickness [mm]	Air Space [mm]	Glass Type	Diameter [mm]
PO-1	Infinity	13.910Cc	7.827	Cemented to PO-2	PBL25Y	4
PO-2	13.910Cx	8.597Cc	3.650	5.844	BSM51Y	4
PO-3	6.090Cx	3.004Cx	9.281	Cemented To PO-4	CaF2	4.5
PO-4	3.004Cc	14.029Cx	10	20.724	BAL15Y	4.5
PO-5	17.316Cx	Infinity	10	4.385(BFD)	PBL6Y	5

The focal ratio conversion optics reimage the fiber ends into a $\sim 1\text{mm}$ long pseudo-slit. Such field size is sufficient to accommodate the 7 fibers of the pupil sliced PRV modes, and an additional sky/calibration fiber, or multiple fibers for the MR or HT modes, Fig. 5.

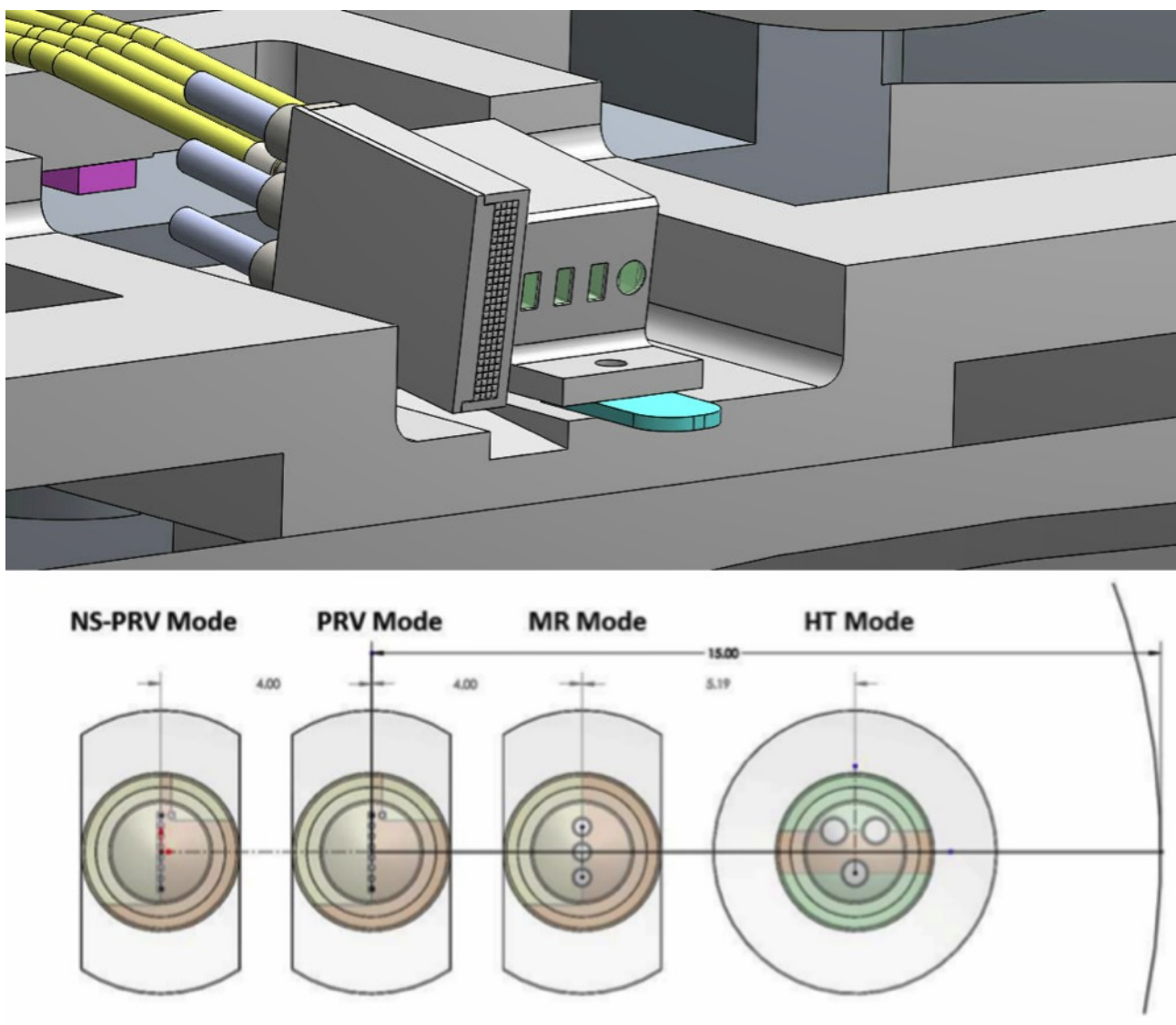


Figure 5: Fiber Feed – Face on view.

G-CLEF main collimator M1, sees an F/8 beam emerging from the pseudo-slit. The fiber end images are located on the optical axis of the collimator at its focus, 2400mm away from the surface vertex point.

Table 5. G-CLEF Collimators

Element	RoC [mm]	Conic	CA [mm]	Comment
M1	4800Cc	Parabolic : -1	500x760	Collimator
M2	3200Cc	Ellipsoidal: -0.97	250x500	Pupil-Transfer Mirror

The collimated beam has a diameter of 300mm, and illuminates an R4 echelle with a groove density of 31.6 lines/mm. The echelle grating is a 306x1200mm mosaic manufactured by Richardson Grating. The location of the grating mid-plane is 2600mm away from the collimator vertex point. The grating face is tilted at 75.96°, and a true Littrow condition is slightly compromised by a 0.75° γ angle (a small clockwise rotation of the grating in the plane of Fig. 1). Therefore, the dispersed beam hits the collimator in second-pass over an elongated area a bit farther away from the optical axis, with respect to the circular first-pass illumination of the white light incoming beam. A footprint diagram of the beam on M1 and the grating is shown in Fig 6.

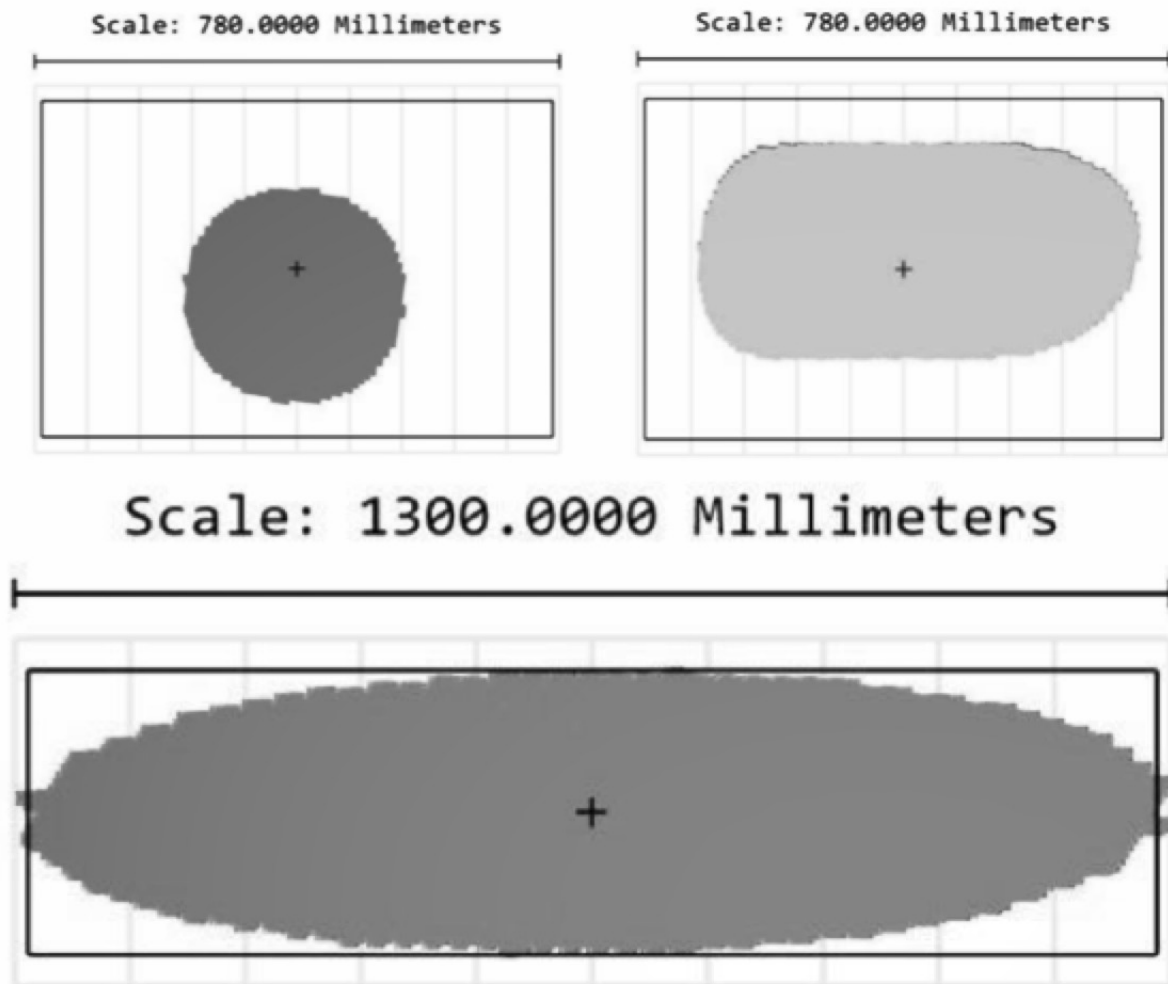


Figure 6: Footprint Diagrams; Left: M1 1st Pass; Right: M1 2nd Pass; Bottom: Echelle Grating Footprint Diagram.

Due to the introduction of the small γ angle of the echelle, the refocused beam clears the slit converging to a point in-between the fiber input and the grating. A Mangin-type fold mirror intercepts the beams reflected from M1 40mm before arriving at an intermediate focus and reflects them towards the pupil-transfer mirror.

The Mangin mirror (Fig. 7 and Table 6) has cylindrical surfaces on its front and back, and serves as the field flattener of the spectrograph. Conventional white pupil designs use a cylindrical field flattener lens in front of the detector. G-CLEF novel solution has the advantage that the field flattener of the cameras can be farther away from the detectors, therefore less prone to ghost image formation [9]. Also, the Mangin mirror provides an overall better correction of field curvature, and allows for the testing of the camera optics without a special field flattener made only for optical testing of the stand-alone camera (*i.e.*, independent of the spectrograph common path optics). The Mangin mirror is wedged and tilted to eliminate a single reflection ghosts discussed further in section 4.

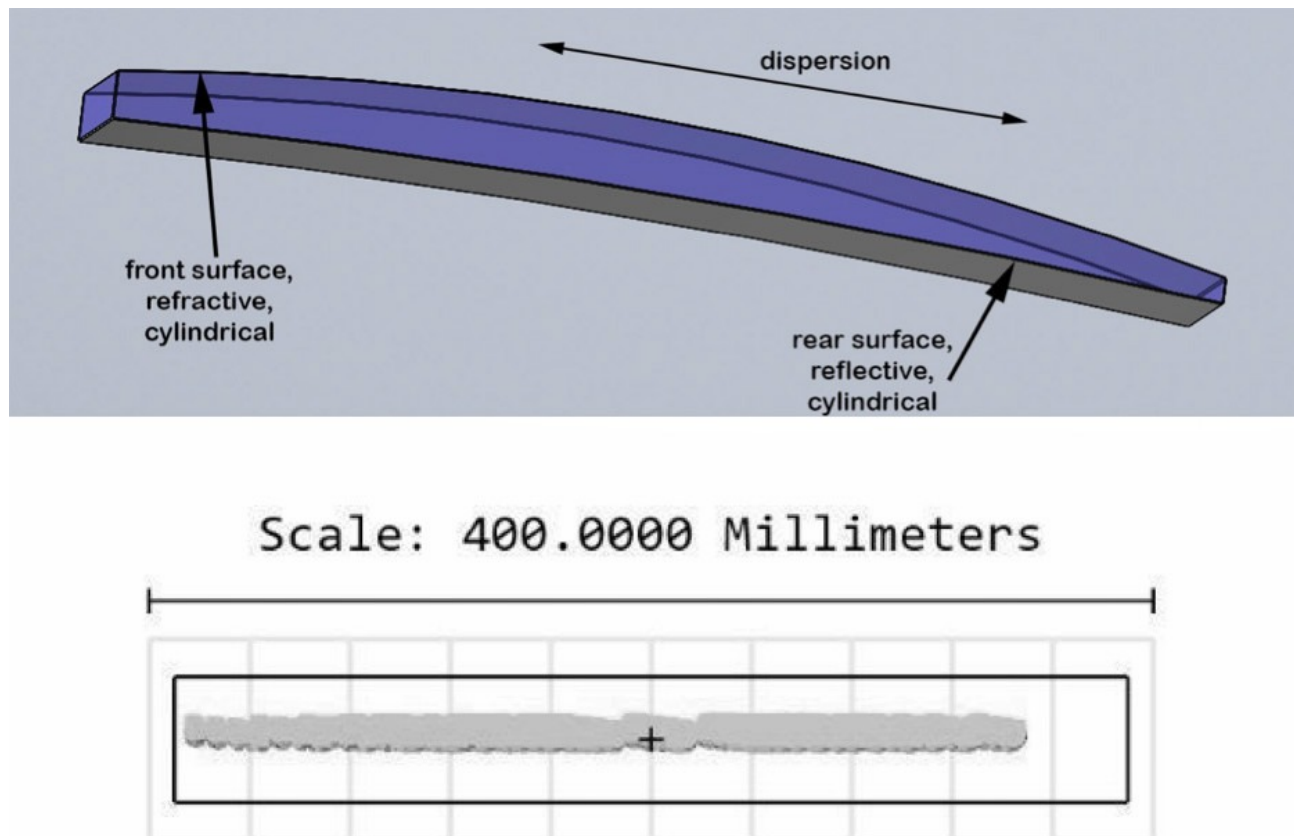


Figure 7: Top: Mangin Mirror Layout; Bottom: Mangin Mirror Footprint (Multi Object Fibers footprint are not shown).

Table 6: Mangin Mirror Optical Prescription.

Element	RoC S1 [mm]	Thickness [mm]	Glass Type	CA [mm]	Remarks
Mangin Front (Refractive)	1053.007Cc	25	Fused Silica	50x380	Toroidal Surface
Mangin Back (Reflective)	3309.726Cc	-	Mirror	50x380	Toroidal Surface

After reflection by the Mangin mirror, the beam is intercepted by a second collimator M2, which has a focal length of 1600mm ($2/3$ the focal length of M1). M2 has a conic constant of -0.97 (*i.e.*, a prolate ellipsoid), with an optical axis in common with that of M1.

Because the focal length of the M2 is less than that of M1, the re-collimated beam has a diameter of $\sim 200\text{mm}$ and therefore permits smaller optical elements down stream (*i.e.*, dichroic, cross disperser and camera lenses). The layout of the spectrograph allows access to the white pupil zone (a conjugate to the pupil on the echelle grating) in its entirety. We chose to put the dichroic before the white pupil, so the cross disperser and a large portion of the camera lenses can be located within the white pupil zone, which is tilted with respect to the local optical axis and thus has a substantial axial extent. This minimizes optical aberrations and achieves more uniform PSF across the echellogram. The dichroic substrate is plane-parallel, 30mm thick fused silica rectangle, with a clear aperture of $255 \times 330\text{mm}$. The dichroic is tilted at 15° with respect to the common optical axes of M1 and M2.

The red cross disperser, located 375mm after the Dichroic back surface, is a VPH grating with a groove density of 480lines/mm , sandwiched between two 20mm thick fused silica plan parallel glass plates. The VPH grating is optimized for the first order at a wavelength of 7300\AA . The imprinted fringes are tilted by 3.25 degrees, so that the VPH grating does not operate in a Littrow configuration and narcissistic ghosts are imaged outside of the detector field of view, see section 4.

The blue cross disperser, located 350mm from the Dichroic front surface, is a grism assembly in which a VPH grating with a groove density of 950lines/mm is sandwiched between two fused silica prisms. The VPH is optimized for the $m=-1$ diffraction order at a wavelength of 4386\AA . The 1^{st} prism has an apex angle of 32.42° while the 2^{nd} prism has an apex angle of 15.87° degrees. The two prisms increase the dispersion for the echelle higher orders with little contribution to the dispersion for lower orders, reducing the gradient in the order spacing for the blue arm. The prisms eliminate the need for tilted fringes in order to avoid VPH ghosts. The VPH gratings are shown in Fig. 8.

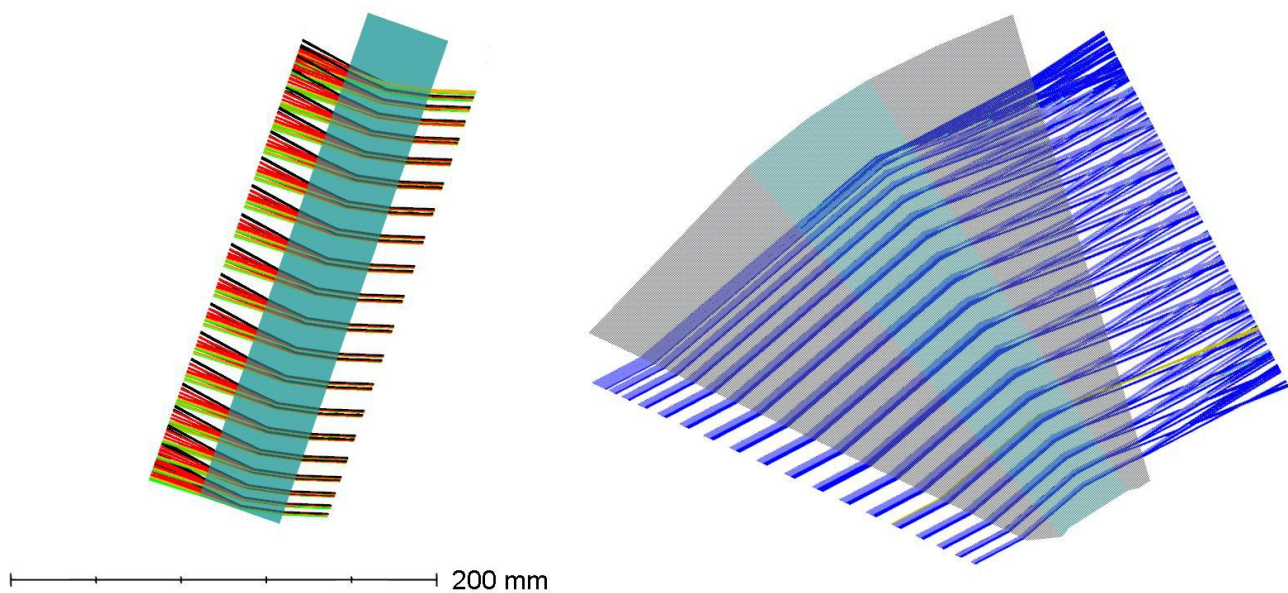


Figure 8: Left: Red VPH Grating; Right: Blue VPH Grism.

2.3 G-CLEF Cameras

The cameras were designed by Harland Epps, and re-optimized by Sagi Ben-Ami in order to maximize performance inside the G-CLEF spectrograph. The field flattener lenses in both cameras are spherical rather than toroidal, made possible because the overall field curvature (in the dispersion direction) introduced by the 2^{nd} reflection from the parabolic collimator M1 has already been compensated by the Mangin mirror.

G-CLEF red camera (Fig. 9 and Table 7) is a 7 element camera with one even-asphere surface (Fig. 10) located on the back surface of the 1st lens. The camera has a focal length of 450mm, beam diameter of 250mm, and a field radius of 7.7°. It is optimized for a wavelength range of 540-950nm, with a small amount of lateral color allowed during optimization.

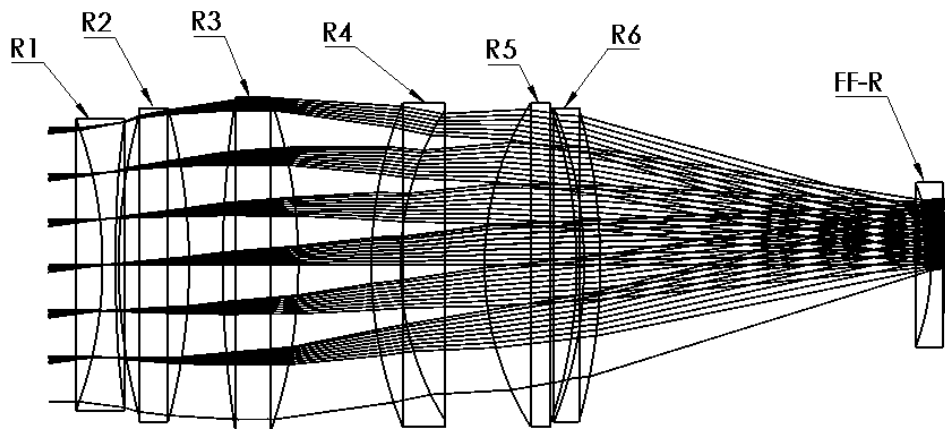
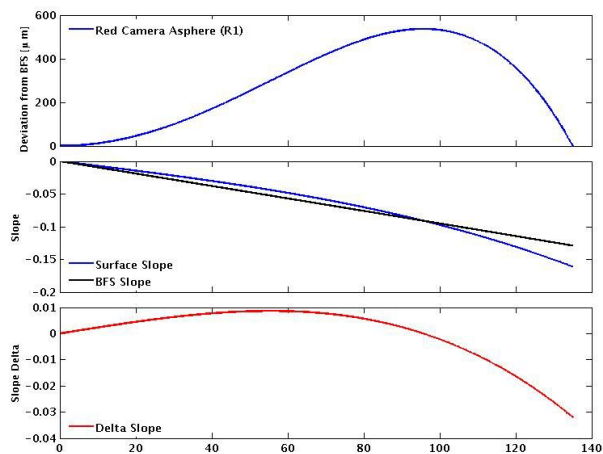


Figure 9: G-CLEF Red Camera.

Table 7: G-CLEF Red Camera Optical Prescription.

Element	RoC S1 [mm]	RoC S2 [mm]	Thickness [mm]	Air Space [mm]	Glass Type	CA [†] S1/S2 [mm]
R1	384.035Cc	1398.150Cc	12	3	BAL35Y	253/265
R2	525.411Cx	552.469Cx	65	31.153	CaF2	282/285
R3	1018.034Cx	474.054Cx	70	67.452	CaF2	305/305
R4	402.072Cc	271.515Cc	27	77.655	PBL25Y	295/286
R5	284.456Cx	458.137Cx	85	7	CaF2	294/288
R6	390.778Cc	540.366Cx	15	305.542	PBM18Y	285/285
FF-R	209.892Cc	3809.379Cx	12	9.958	S-BAH27	126/126

[†] Clear Aperture



RoC	1398.150mm (Cc)
BFS	1054.585mm
a4	6.308×10^{-9}
a6	9.484×10^{-15}
a8	-8.183×10^{-20}

Figure 12: G-CLEF Red Camera Aspheric Surface Characteristics.

G-CLEF blue camera (Fig. 11 and Table 8) is an 8 element camera with one even-asperse surface (Fig. 12) located on the back surface of the 1st lens. The camera has a focal length of 450mm, beam diameter of 260mm, and a field radius of 6.5 degrees. It is optimized for a wavelength range of 350-550nm, with a small amount of lateral color allowed during optimization.

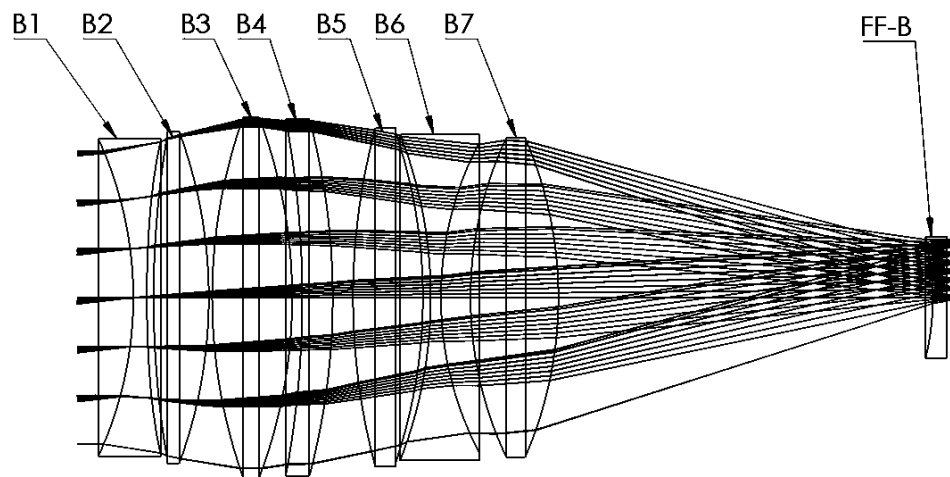
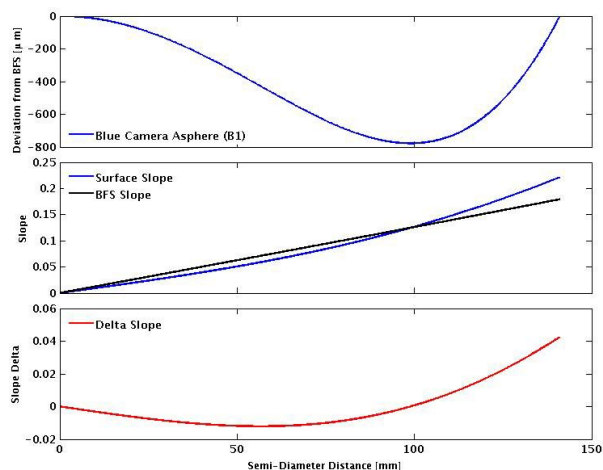


Figure 11: G-CLEF Blue Camera.

Table 8: G-CLEF Blue Camera Optical Prescription.

Element	RoC S1 [mm]	RoC S2 [mm]	Thickness [mm]	Air Space [mm]	Glass Type	CA ⁴ S1/S2 [mm]
B1	334.625Cc	1076.159Cc	12	6	BAL35Y	264/277
B2	856.795Cx	425.428Cx	49	3	CaF2	284/289
B3	478.163Cx	449.796Cx	71	9	CaF2	315/315
B4	856.806Cx	613.209Cx	27	18	PBM18Y	311/311
B5	577.663Cx	454.92Cx	62	7	CaF2	295/290
B6	398.297Cc	295.078Cc	9	26.3	BAL35Y	284/272
B7	331.723Cx	354.031Cx	78	332.322	CAF2	280/280
FF-B	224.438Cc	2836.237Cc	12	9.38	BSM51Y	108/108

⁴Clear Aperture



RoC	1076.159mm (Cc)
BFS	799.472mm
a4	8.569×10^{-9}
a6	-7.207×10^{-15}
a8	-4.809×10^{-19}

Figure 12: G-CLEF Blue Camera Aspheric Surface Characteristics.

Both the red and blue cameras show excellent image quality, with 80% ensquared energy below 18 μ m for all point sources in the spectrograph slit across all modes. The energy fraction in a single resolution element for the PRV and MR mode is given in Fig. 13 (the resolution is determined by the echelle grating and the fiber core diameter).

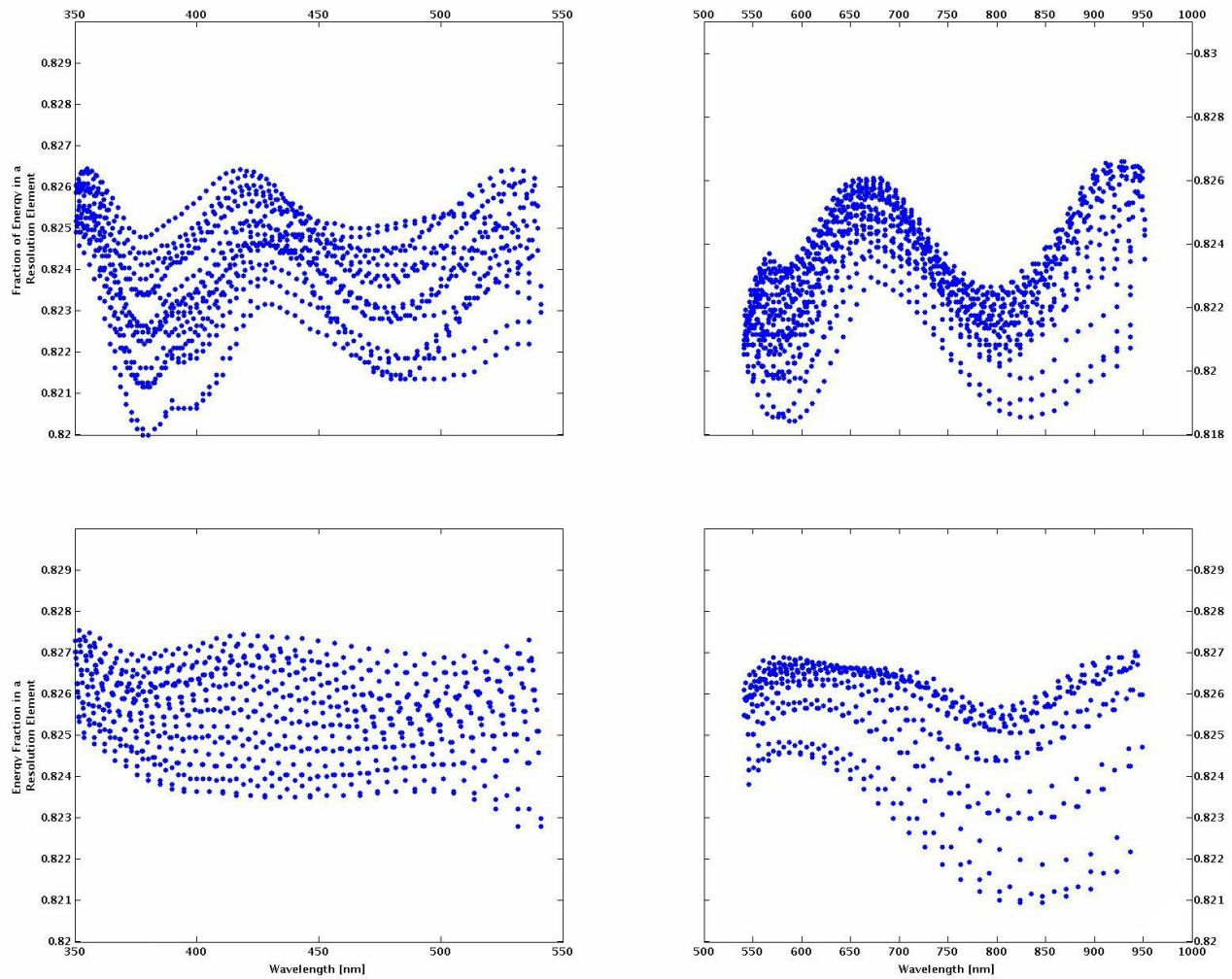


Figure 13: Ensquared Energy per resolution elements. Left: Blue Camera; Right: Red Camera; Top: PRV Mode; Bottom: MR mode.

The image quality in a stand-alone mode (*i.e.*, cameras are fed by collimated light) is shown in Fig. 14, demonstrating the testability of the cameras independent of other optical elements in the spectrograph.



Figure 14: Camera performance outside of the Spectrograph mainframe. Left/Right: Blue/Red Camera; Box size=100µm.

3. ECHELLOGRAMS

The blue/red echellogram is imaged onto a 95.04×95.04mm (92.4×92.2mm) STA (e2V) monolithic detector, with a 9µm (10µm) pixel size.

While the spatial length of each order on the detector (*i.e.*, the dispersion direction) is determined by the free spectral range, the target resolution, slit width, and camera focal length, the VPH grating/grism govern the height of the echellogram (*i.e.*, in the cross-dispersion direction). When determining the cross-disperser parameters, we consider the following criteria:

1. A large enough inter-order spacing to keep order blending at less than <1%.
2. A large enough intra-order spacing to keep fiber image blending at less than <1% (This is determined by the 7+1 fibers imaged in the PRV mode).

These two criteria benefit from the large CCD format and full use of the imaging surface, with a reasonable margin to allow easy alignment of the detector.

After a rigorous optimization, we find that the VPH grating/grism parameters given in section 2 are the optimum parameters given the two criteria above. For the red (blue) echellogram, we get a minimum inter-order separation of 210µm (244µm) and a minimum intra-order separation of 120µm (110µm), see Fig. 15 and 16.

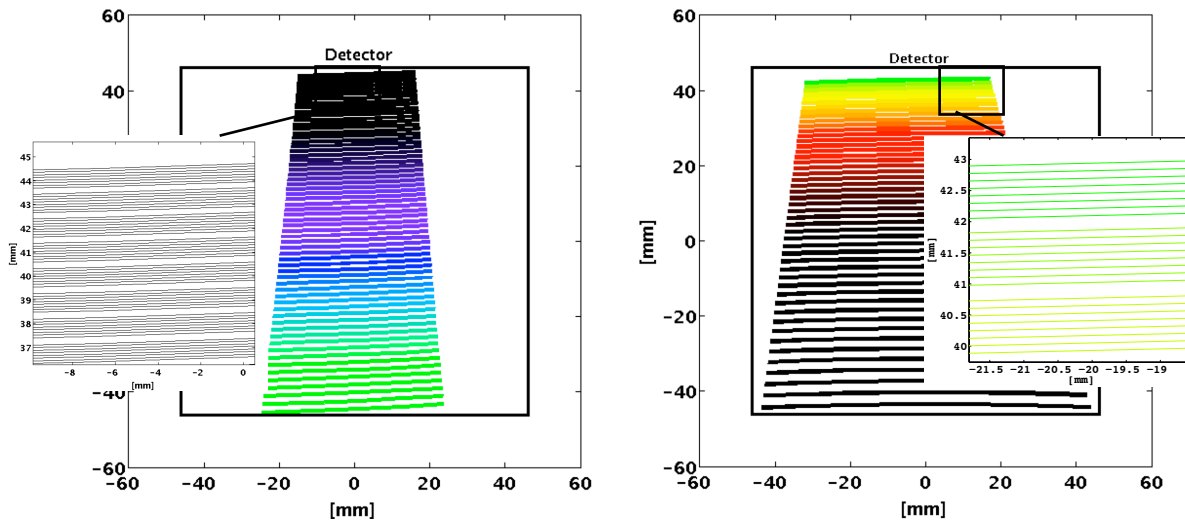


Figure 15: PRV Echellograms. Left: Blue; Right: Red.

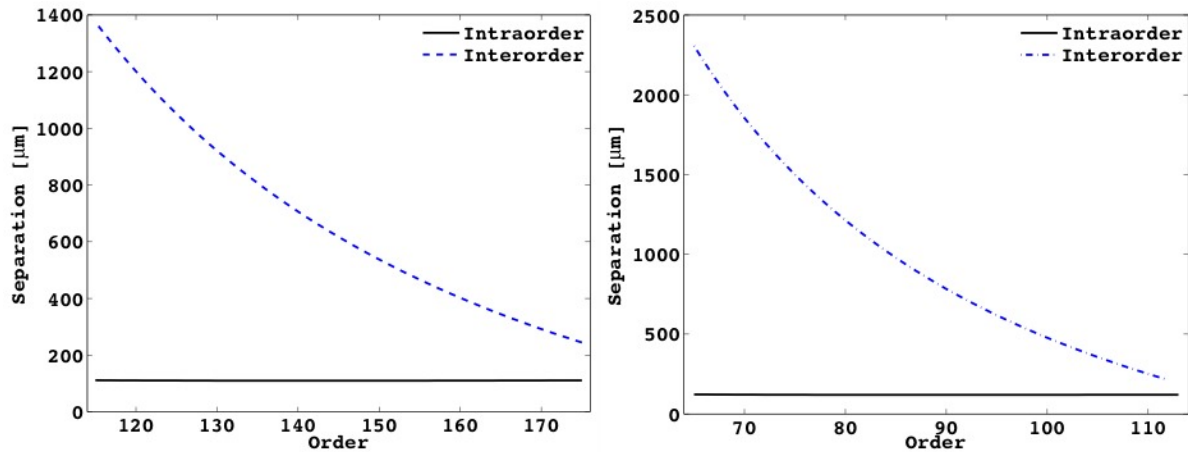


Figure 16: Inter/Intra-Order Separation. Left: Blue; Right: Red.

4. EXPOSURE METERS

In order to obtain radial velocity measurement accuracy of several meter per second and below, it is necessary to correct the measured line of sight velocity to the Solar System barycenter [11]. In order to apply this correction, we need to get an exact measurement of the photo-center exposure (*i.e.*, the intensity-weighted time at which the exposure was taken). When aiming at a PRV accuracy of $\geq 10\text{cm/s}$, the wavelength dependency of this barycentric correction might also play a role.

In order to determine the photo-center of each exposure, G-CLEF utilizes two exposure meters, one located in each of the spectrograph arms. A finite amount of photons are scattered by the VPH grating/grism into the $m = 0$ order (roughly 5%; Private correspondence with Kaiser Optical Systems). A pickup mirror inside the camera reflects these onto an exposure meter located above the camera mounts, Fig. 17. The exposure meters are large multianode photocathodes with a photo sensitive area of $30 \times 30\text{mm}$ allowing us to introduce several filters simultaneously.

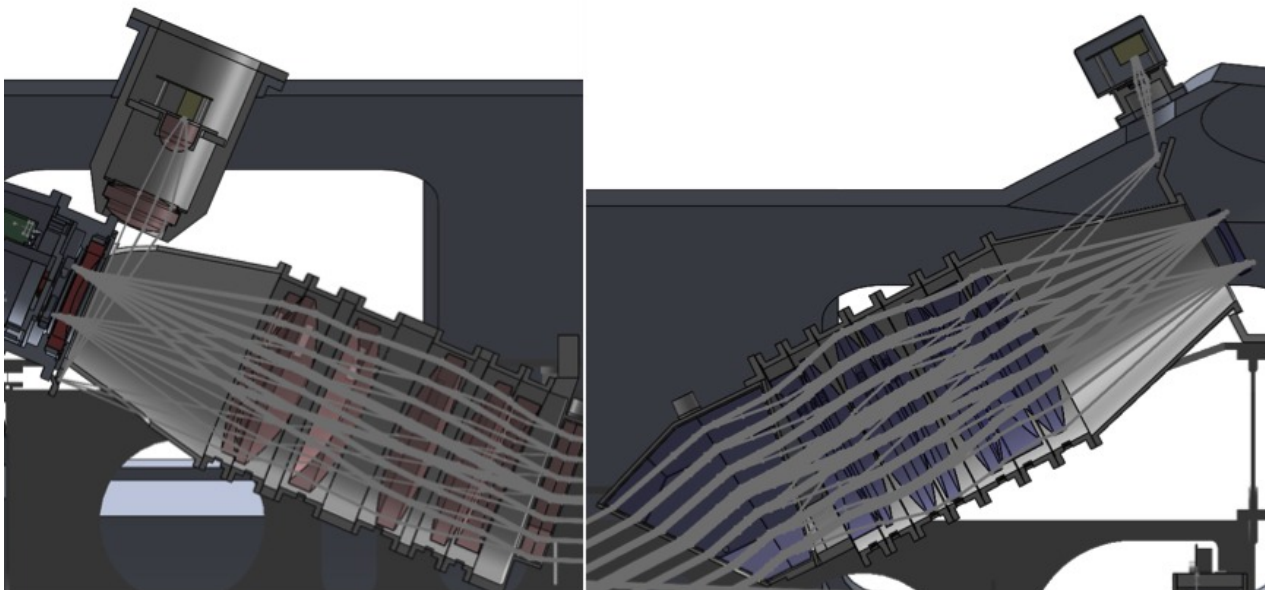


Figure 17: Left: Red Arm Exposure Meter; Right: Blue Arm Exposure Meter.

5. GHOST ANALYSIS

5.1 Mangin Mirror

The Mangin mirror is a reflective optical element located in proximity to the intermediate focal plane generated by M1 2nd pass reflection. The OPD between rays reflected from the front surface (or rays reflected in the glass-to-air interface) and the chief ray is of $\mathcal{O}(10)mm$, and therefore will produce ghost images at an intensity of $\sim 1\%$ (The AR coating efficiency of the front surface), see Fig. 18 left panel. In order to mitigate these single reflection ghost images, we introduce a wedge to the Mangin mirror front surface, as well as a tilt to the entire element, which cause the rays associated with the ghost images to miss the optical elements downstream. The tilt angle (1.375°) is exactly half of the wedge angle (2.75°), so that the original rays are not affected by this method, see Fig 18 right panel.

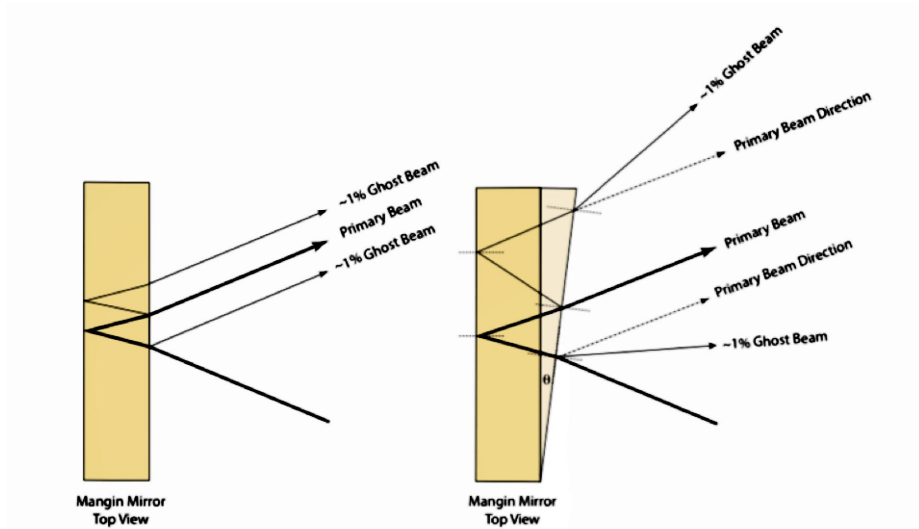


Figure 18: Left: The Mangin mirror will generate ghost images at an intensity of $\sim 1\%$; Right: A small Wedge and tilt of the Mangin mirror mitigates this problem.

5.2 VPH Grating/Grism

Several instruments using VPH gratings have shown a significant amount of ghost images generated by back-reflections from these gratings [12]. Although this phenomenon is not unique to VPH gratings, it is more perilous in this type of disperser because of their structure, in which a gelatin layer is sandwiched between two flat glass surfaces. While this problem is avoided in the blue VPH grism due to the presence of a prism, the red VPH might introduce a significant amount of ghost images on the spectrograph focal plane.

In general, we divide VPH ghosts into two types:

Narcissistic Ghosts: Scattering from Gelatin-Glass interface after reflection from the detector ($m = 1$; $m' = 0$).

Littrow ghost: Recombination of cross dispersed orders by the VPH ($\Delta m = 0$).

We mitigate VPH ghost images in the red arm by introducing a tilt to the imprinted fringes, which move the operation wavelength away from the Littrow configuration. The fringe tilt is large enough so that the ghosts are moved away from the detector, Fig. 19.

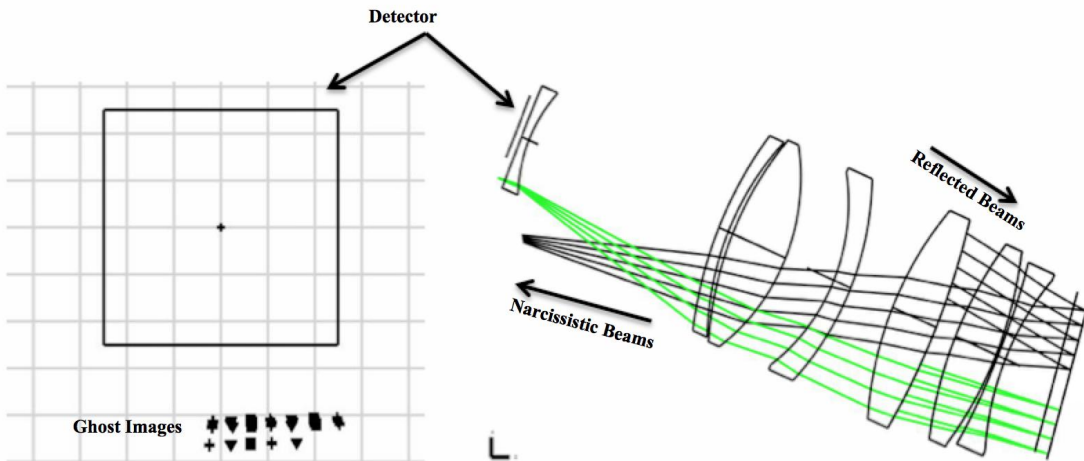


Figure 14: The VPH tilted fringes causes beams reflected by the detector to back-scatter at higher angles, outside of the detector field-of-view.

5.3 Blue/Red Camera

A ghost analysis shows that for the blue and red camera pupil ghosts are at a level of $< 10^{-12}$ per pixel, while focused ghosts images are at a level of $\mathcal{O}(10^{-9})$, both orders of magnitude below the detector full well capacity, $\mathcal{O}(10^5)$.

6. SUMMARY

G-CLEF, is a high-resolution optical echelle spectrograph with a PRV capability. Its optical design incorporates novel techniques to allow 10cm/s precision radial velocity measurements without sacrificing other capabilities such as various resolution modes and throughput. The post PDR design presented takes into account considerations such as inter- and intra-order contamination, ghost images by various optical elements, and the need for a multi-color exposure meter. G-CLEF is currently in a critical design phase, with estimated delivery in 2021 as the 1st light instrument for the GMT.

The authors would like to thank to Gabor Furesz and Stuart I. Barnes for their kind advice and contribution to the project. The authors would also like to thank the G-CLEF and GMT team for their support and collaboration throughout the project phases.

REFERENCES

- [1] Baranne & Duchesne, *Auxiliary Instrumentation for Large Telescopes*, 241, 1972.
- [2] Dekker, Delabre & Dodorico, *Proc. of the International Society for Optical Engineering*, 627, 339, 1986.
- [3] Lawrence J. S., et al., "The MANIFEST prototyping design study", *Proc. SPIE 9908*, Ground-based and Airborne Instrumentation for Astronomy VI (2016).
- [4] Szentgyorgyi, A. et al., "The GMT-Consortium Large Earth Finder (G-CLEF): an optical Echelle spectrograph for the Giant Magellan Telescope (GMT)", *Proc. SPIE 9908*, Ground-based and Airborne Instrumentation for Astronomy VI (2016).
- [5] Baldwin, D. et al., "Advanced Structural Design for Precision Radial Velocity Instruments", *Proc SPIE 9912*, Ground-based and Airborne Instrumentation for Astronomy VI (2016).

- [6] Evans, I. N., et al., "Software requirements flowdown and preliminary software design for the G-CLEF spectrograph", *Proc. SPIE* 9913, Ground-based and Airborne Instrumentation for Astronomy VI (2016).
- [7] Muller, M. A., et al., "The opto-mechanical design of the GMT-Consortium Large Earth Finder (G-CLEF)", *Proc. SPIE* 9908, Ground-based and Airborne Instrumentation for Astronomy VI (2016).
- [8] Oh, J. S., et al., "Opto-mechanical design of the G-CLEF flexure control camera system", *Proc. SPIE* 9908, Ground-based and Airborne Instrumentation for Astronomy VI (2016).
- [9] Furesz, G. et al., "The G-CLEF spectrograph optical design", *Proc. SPIE* 9147, Ground-based and Airborne Instrumentation for Astronomy V (2014).
- [10] Crane, J. et al., "G-CLEF Front-End Optics", in prep.
- [11] Wright, J. T. and Eastman, J. D., "Barycentric Corrections at 1 cm s^{-1} for Precise Doppler Velocities", *Publications of the Astronomical Society of the Pacific*, 126, 838-852 (2014).
- [12] Burgh E. B., et al., "Recombination Ghosts in Littrow Configuration: Implications for Spectrographs Using Volume Phase Holographic Gratings", *Publications of the Astronomical Society of the Pacific*, 119, 1069-1082 (2007).